Macromolecules

ARTICLE

pubs.acs.org/Macromolecules

In Situ Synchrotron SAXS Study of Polymerizable Microemulsions

Shuhua Peng,[†,‡] Qipeng Guo,[*,†] Timothy C. Hughes,[‡] and Patrick G. Hartley[*,‡]

[†]Institute for Technology, Research and Innovation, Deakin University, Geelong, Victoria 3217, Australia

[‡]CSIRO Materials Science and Engineering, Bayview Avenue, Clayton South, Victoria 3169, Australia

Supporting Information

ABSTRACT: We present for the first time a real-time small-angle X-ray scattering (SAXS) study of the structural transition of fluid microemulsion to solid polymerized material in a silicone polymerizable microemulsion system. A reactive methacrylate-terminated siloxane macromonomer (MTSM, $M_n \sim$ 1000 g/mol) was synthesized and used for microemulsion formulations comprising MTSM (oil phase), water, and a mixture of nonionic surfactant (Teric G_9A_8) with isopropanol. *In situ* synchrotron SAXS was used to investigate time-dependent nanostructure evolution during the polymerization reaction, which was directly initiated by X-ray radiation. The SAXS data were analyzed using both the Teubner−Strey model and the core−shell model. The results obtained by the Teubner−Strey model showed that the domain size (d) decreased while the correlation length (ξ) increased upon polymerization. The analysis in terms of the core−shell model displayed that adding water to the precursor microemulsion caused the water droplets to start swelling, which resulted in the discontinuity of water in oil microemulsion. There exhibited large differences in morphologies of polymerized materials from the microemulsion formulations with different water and surfactant contents. The core and shell sizes of water droplets decreased during the course of polymerization when there was 15 wt % or more water in the microemulsion formulation; the polymerized material thus exhibited increasingly discrete granular morphology. When there was 10 wt % or less water content in the precursor microemulsion, the rearrangement of water domains could be minimized during the course of polymerization and transparent polymerized material was obtained.

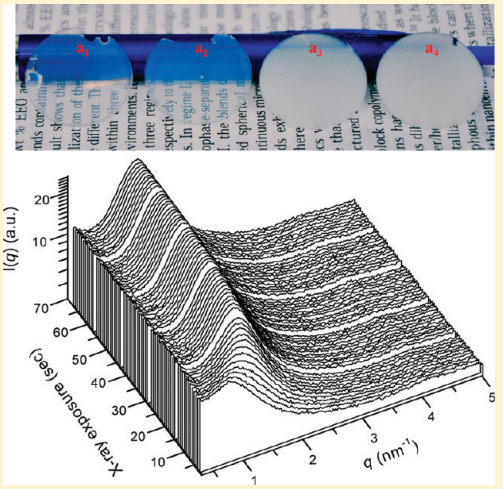

INTRODUCTION

Microemulsions are thermodynamically stable, nanostructured dispersions of two immiscible liquids such as oil and water stabilized by a surfactant or by a surfactant/cosurfactant mixture.[1] They are isotropic, optically transparent, usually have low viscosity, and are used as the basis for formulations used in consumer products, pharmaceutical, and petroleum recovery applications, to name but a few. Microemulsions exhibit rich nanostructural diversity, and they have been successfully applied as templates for the production of nanoporous materials via organic and inorganic polymerization reactions.[2−4] In general, the use of microemulsions as templates should lead to materials with a high surface area and a structure reminiscent of the microemulsion template. These materials may be suitable for a range of applications that require high surface area and permeability (e.g., separations and catalysis).[3,5] Specifically, polymerizable inverse microemulsions can be used to synthesize high molecular weight water-soluble polymer particles[6] while polymerizable bicontinuous microemulsions allow the production of porous sponge like polymer solids which can be used as membranes in separation applications.[7]

There has been significant effort to employ polymerizable microemulsions to prepare well-defined porous materials for other technological applications.[8−12] For instance, transparent polymeric materials without inorganic filler have been produced by the polymerization of bicontinuous microemulsions containing polymerizable surfactants for use in biomaterials/ophthalmic applications.[11] The pore size of the polymer films was regulated by the composition of the precursor bicontinuous microemulsions. A limited number of studies have demonstrated the ability to carry out microemulsion polymerization for synthesis of polymeric materials with well-defined nanometer-sized structure. For example, Co et al.[13−15] have developed an approach using solid microemulsion glasses as templates to overcome such structural rearrangement and generated highly ordered porous materials. However, more often than not, the final polymerized material seldom reflects the starting template microstructure.

It is generally accepted that the nanostructure of the precursor microemulsion is a critical determinant of the nanoporosity of the final material[11,16,17] and that control over the size and shape of the resulting structure can be manipulated by controlling the microemulsion phase behavior, yet there remains a considerable gap in knowledge concerning the relationship between the

Received: December 31, 2010
Revised: March 14, 2011
Published: March 30, 2011

Scheme 1. (a) Structure of Hydroxyl-Terminated PDMS and (b) Synthesis Route of MTSM

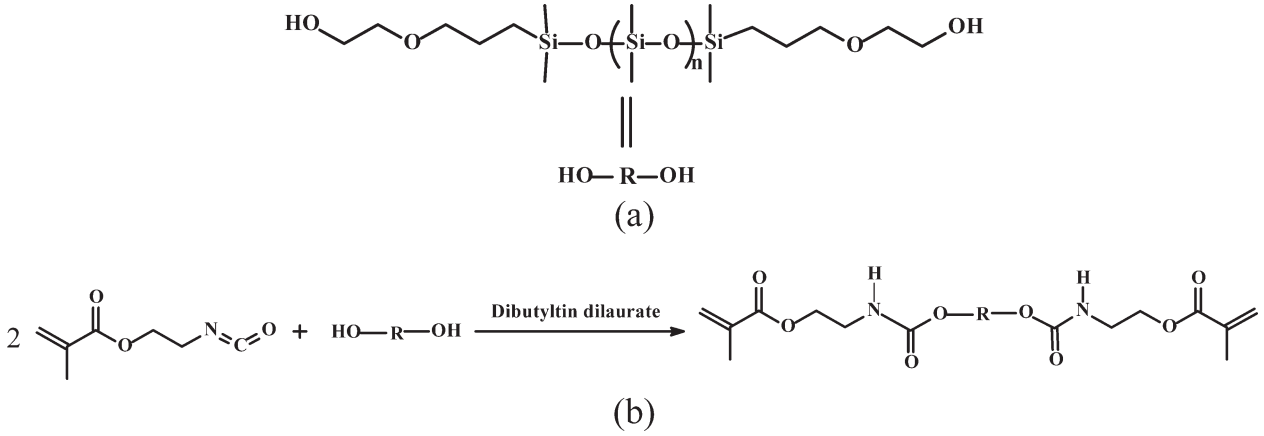

template microemulsion nanostructure and the final nanoporous polymerized material. This is because the microemulsion structure evolves continuously during the polymerization process as a result of the compositional and volume changes caused by the consumption of monomer. In some cases,[8,9] a phase separation occurs during the microemulsion polymerization. Although there have been several studies[17−19] demonstrating the ability of minimizing the rearrangement and phase separation during the microemulsion polymerization by use of the polymerizable surfactants, little work[20,21] has been reported to describe the relationship between the microstructures of polymerizable microemulsion systems and the final polymerized morphologies and/or the solution nanostructural transitions which occur during microemulsion polymerization reactions. In order to obtain better control over the size and shape of the resulting structure during the microemulsion polymerization,[6,22] a clear understanding of the structural rearrangements which occur during the polymerization process is required.

Thus, the goal of this work was to develop a route for the preparation of controlled polymer morphologies based on tuning precursor microemulsion phase behavior. We have developed an inverse microemulsion system comprising an oil phase based on a polymerizable siloxane macromonomer, water, and a mixture of a nonionic surfactant (Teric G_9A_8) and isopropanol (IPA). A reactive methacrylate-terminated siloxane macromonomer (MTSM, $M_n \sim 1000$ g/mol) was synthesized and used as the oil phase in the microemulsion. The single-phase region of the ternary phase diagram was partially mapped for a fixed weight ratio 4:1 of surfactant and IPA. Microemulsion polymerization was initiated by either ultraviolet (UV) or X-ray radiation through the introduction of a photoinitiator. The rapid polymerization allowed experiments to be performed in a few minutes. The time evolution of nanostructural changes during the course of polymerization were directly investigated by *in situ* synchrotron small-angle X-ray scattering (SAXS). The final morphology of the polymerized material was investigated by scanning electron microscopy (SEM). On the basis of the analysis of the data, a conceptual model was proposed to describe the relationship between the starting microemulsion phase behavior and the final polymer nanostructure. Importantly, this should enable specific polymer properties to be targeted based on the starting microemulsion composition and nanostructure.

EXPERIMENTAL SECTION

Materials. Bis(2-hydroxyethyl propyl ether)-terminated poly(dimethylsiloxane) (hydroxyl-terminated PDMS) (X-22-160AS, M_w = 1067 g/mol) was purchased from ShinEtsu Chemical Co. Ltd., and it was dried using 4 Å molecular sieves for at least 24 h before use. 2-Isocyanatoethyl methacrylate (IEM), purchased from Amtrade International Pty. Ltd., was purified by distillation under reduced pressure and stored in a closed vessel under dark condition at −20 °C prior to use. Dibutyltin dilaurate (DBTDL) and isopropanol (IPA) from Merck Co.; Teric G_9A_8 from ICI Australia Operations Pty. Ltd.; and photoinitiator (Darocur 1173) from Sigma were used as received. The polypropylene molds used for casting and UV polymerization of microemulsions were supplied by Ciba Vision Corp. The flat polypropylene molds had a diameter of 20 mm and a thickness of 100 μm.

Synthesis of Methacrylate-Terminated Siloxane Macromonomer (MTSM). MTSM was prepared by an adaptation of the method reported in the literature,[23,24] and the synthesis route is shown in Scheme 1. In a typical experiment, hydroxyl-terminated PDMS (12.0 g, 0.012 mol) and IEM (4.0 g, 0.026 mol) were added into a round-bottom flask fitted with a Teflon-coated magnetic stirrer bar. The flask was sealed and stirred vigorously to produce a homogeneous solution. After 10 min, the catalyst DBTDL (20 μL) was added into the flask, and the solution was stirred for another 24 h to ensure a complete reaction in the absence of light at room temperature. In order to purify MTSM, 50 mL of toluene as dilution agent was added into the mixture, and then the mixture was washed with deionized water repeatedly to remove the catalyst and the unreacted IEM through a separating funnel. After drying with anhydrous sodium sulfate, the upper layer solution of MTSM was treated by filtration and evaporation under reduced pressure to remove toluene and the purified MTSM was obtained. Proton nuclear magnetic resonance (^{1}H NMR) spectra of MTSM were recorded on a Bruker NMR spectrometer at 400 MHz using deuterated chloroform as the solvent. ^{1}H NMR chemical shifts (δ) in parts per millions (ppm) were referenced relative to chloroform (δ = 7.26 ppm) as an internal standard.

Determination of Microemulsion Phase Diagram. The partial quasi-ternary phase diagram of the MTSM−water−Teric G_9A_8/IPA mixture system at 25 ± 0.2 °C was determined by direct observation of the changes from transparency to turbidity. First, different ratios of MTSM and Teric G_9A_8/IPA were prepared in the culture tubes. The phase-separation boundary curve was then obtained via water titration of the one-phase mixtures of MTSM and Teric G_9A_8/IPA until turbidity was observed. The samples were thoroughly mixed after each addition of water using a Vortex mixer. The transparent single-phase region was established from the clear-turbid boundaries based on systematic titrations.

Small-Angle X-ray Scattering (SAXS). SAXS experiments were performed at the Australian Synchrotron on the small/wide-angle X-ray scattering beamline utilizing an undulator source that allows measurement at a very high flux to moderate scattering angles and a good flux at the minimum q limit (0.012 nm^{-1}). The wavelength λ of X-ray was 0.062 nm, and the scattering curves were monitored in a q-range from 0.2 to 11 nm^{-1}. The magnitude of the scattering vector (q) is defined as[25]

$$q = \frac{4\pi}{\lambda}\sin\left(\frac{\theta}{2}\right) \quad (1)$$

where λ is the wavelength of the X-ray and θ is the scattering angle. The samples were inserted into 1.0 mm quartz capillaries which were then sealed. The background correction was performed by measuring the scattering of an empty capillary and correcting for sample absorption. The SAXS data were analyzed by fitting to model expressions (Teubner−Strey and core−shell model) using the program SansView developed by the University of Tennessee.[26] The scattering caused by microemulsion structure ends around $q \sim 5.0$ nm^{-1}, and afterward the tails of the SAXS curves leveled off. The SAXS data fitting was performed in the area of interest $0.3 < q < 5$ nm^{-1}.

Microemulsion Polymerization by UV. Microemulsion formulations were polymerized using 2 wt % photoinitiator Darocur 1173, which was based on the weight of MTSM. The weight ratio of Teric G_9A_8/IPA was always maintained at 4:1. For SAXS measurements, the precursor microemulsion solution was first loaded into 1.0 mm quartz capillaries, and then the sealed capillaries were put into the UV box for polymerization. For polymer morphology studies, the microemulsion solution was casted into the polypropylene molds, and following photopolymerization, the resultant polymer membranes were fractured for SEM imaging. In this case, photopolymerization was carried out in a UV box working at a wavelength of 365 nm (with an output of 10 mW/cm^2) for about 10 min at room temperature.

***In Situ* Monitoring of Polymerization Process by SAXS.** To determine how the structure of the microemulsion developed during the polymerization process, microemulsion solutions were polymerized *in situ* using X-ray radiation from synchrotron SAXS beamline. Microemulsion precursor solution samples were injected into 1.0 mm capillaries. The precursor solutions were exposed to X-ray radiation at $E = 20$ keV in a series of 1 s exposures. This allowed scattering data to be collected during polymerization so that the structural transitions occurring during the transition from a microemulsion solution containing PDMS macromonomer to a cross-linked PDMS network could be followed. After exposure to a sufficient amount of X-ray radiation, the part of transparent microemulsion solution under X-ray radiation for some formulations gradually became opaque, indicating that polymerization had occurred. It has previously been shown that X-ray radiation can initiate the polymerization of an acrylamide functionality in the similar manner as UV radiation.[27,28] *In situ* polymerization generally exhibited well-defined SAXS patterns which correlated well with those obtained from UV-polymerized samples.

Scanning Electron Microscopy (SEM). The morphology of polymerized materials was examined with a field emission scanning-electron microscopy (FE-SEM, Philips, XL30). While the samples for real-time SAXS study were directly initiated by synchrotron X-ray polymerization, the ones for SEM study were cured by UV (see the Supporting Information). However, the SAXS patterns for the samples prepared by different methods (Figure S1) are almost the same, and the differences of the structure are negligible. The polymerized microemulsion samples were fractured mechanically after being frozen in liquid nitrogen. The fractured samples were vacuum-dried for 24 h at room temperature and then coated with gold for SEM analysis.

RESULTS AND DISCUSSION

Synthesis and Characterization of MTSM. The MTSM macromonomer contains reactive methacrylate groups at both ends such that it can be cross-linked without adding external curing agent. The ^{1}H NMR spectrum of MTSM is shown in Figure 1. The simultaneous appearance of resonances characteristic of both IEM and hydroxyl-terminated PDMS indicates that MTSM macromonomer was successfully obtained. All of the methyl protons in the silicone segments ($-Si(CH_3)_2-O-$) appeared together close to at 0.0 ppm. Chemical shifts corresponding to the methylene protons j, i, h, g, and f of PDMS were found at 1.76, 1.59, 3.38, 3.47, and 4.18 ppm, respectively. Other signals in the IEM spectrum at 1.90 ppm (a), 6.07 and 5.55 ppm (b), 3.58 ppm (c), 4.18 ppm (d), and 5.13 ppm (e) were also identified, and they confirmed the successful end-group functionalization reaction of PDMS.

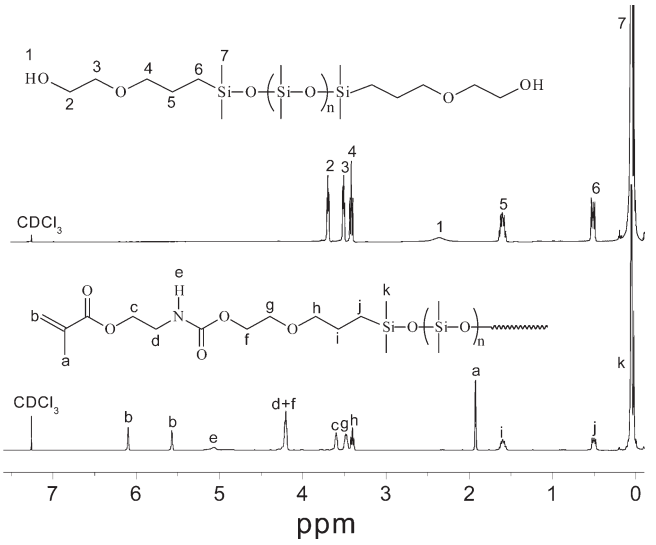

Figure 1. ^{1}H NMR spectra of the MTSM in $CDCl_3$.

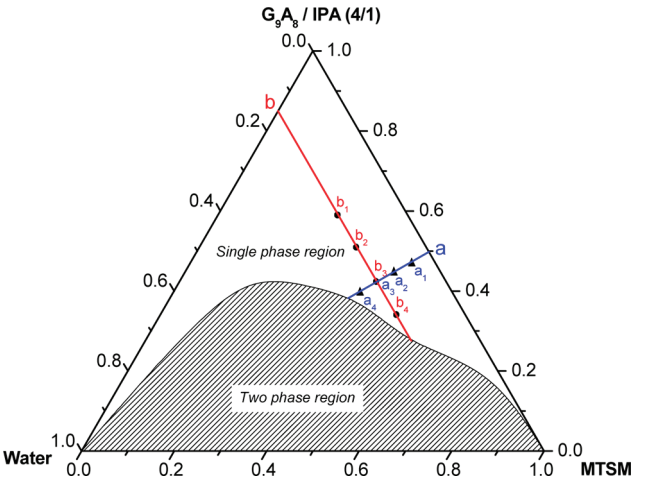

Figure 2. Phase diagram of the MTSM/water/Teric G9A8/IPA at 25.0 ± 0.2 °C (weight fraction).

Phase Behavior of Microemulsions. The highly hydrophobic character of silicone systems tends to make the preparation of polydimethylsiloxane microemulsions difficult.[29,30] Hence, the one-phase region of the phase diagram for the MTSM systems was partially mapped for a fixed weight ratio 4:1 of Teric G_9A_8 to IPA (Figure 2). The domain located below the phase boundary curve corresponds to a two-phase region (shaded domain),

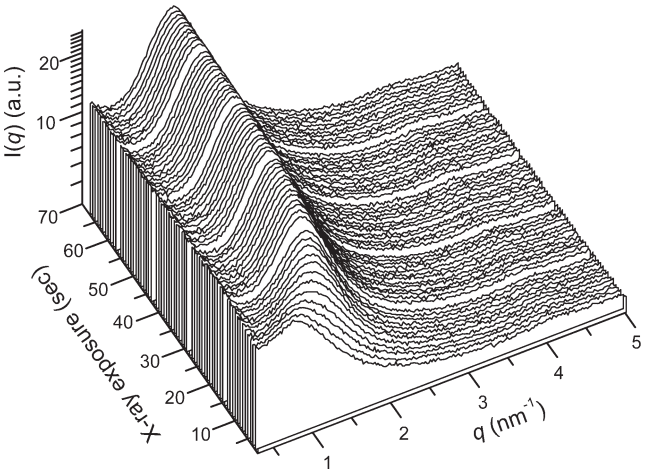

Figure 3. Time dependence of SAXS intensity $I(q)$ during microemulsion polymerization under X-ray at room temperature. Microemulsion composition (b_4): 15 wt % water, 51 wt % MTSM, and 34 wt % surfactant.

whereas that above represents the single-phase region. A single water dilution line (a) and a constant water content line (b) were indicated in the phase diagram for the following SAXS and SEM measurements. These two lines were selected for detailed examination because of the high MTSM content and significant morphological differences between them after polymerization.

SAXS during *in Situ* Microemulsion Polymerization. Figure 3 shows the evolution of scattering curves during X-ray-induced photopolymerization of an MTSM macormonomer microemulsion (57 wt %) at 25 °C. The data were recorded on the SAXS beamline of the Australian Synchrotron. As X-ray exposure time increases, a qualitative change in the scattering behavior of microemulsion solution occurred as a result of nanostructural rearrangement upon polymerization. Initially, it exhibited a typical SAXS pattern from microemulsion system, and a single broad scattering peak was observed. After exposure to X-ray radiation for a few seconds, the single broad peak became sharper and shifted toward higher q. The q_{max} position of the peak did not change any further after 30 s of X-ray radiation, while the peak intensity continued to increase up to 40 s exposure. These results imply that most polymerization occurred in the first 30 s and that the structure of the microemulsion changed monotonically and rapidly during the polymerization process.

For SAXS analysis of the global structural properties of microemulsions, Teubner and Strey[31] developed a phenomenological model which has been widely used to describe scattering from aqueous microemulsions stabilized by nonionic surfactant.[14,21,32−34] Lodge and co-workers also have extended this model for structured polymer blends.[35−37] This model uses three fitting parameters to describe the observed broad scattering peak, and the function takes the form

$$I(q) = \frac{1}{A + Bq^2 + Cq^4} \tag{2}$$

In eq 2, the constraints that A, B, and C are variables which can be obtained by nonlinear least-squares fitting of the experimental data. The physical parameters d and ξ, representing the domain size (periodicity of the oil and water domains) and correlation length (which describes the decay length of the periodic order) present in the microemulsions, respectively, are related to the constants in eq 2:

$$d = 2\pi\left[\frac{1}{2}\left(\left[\frac{A}{C}\right]^{1/2} - \frac{B}{2C}\right)\right]^{-1/2} \tag{3}$$

$$\xi = \left[\frac{1}{2}\left(\left[\frac{A}{C}\right]^{1/2} + \frac{B}{2C}\right)\right]^{-1/2} \tag{4}$$

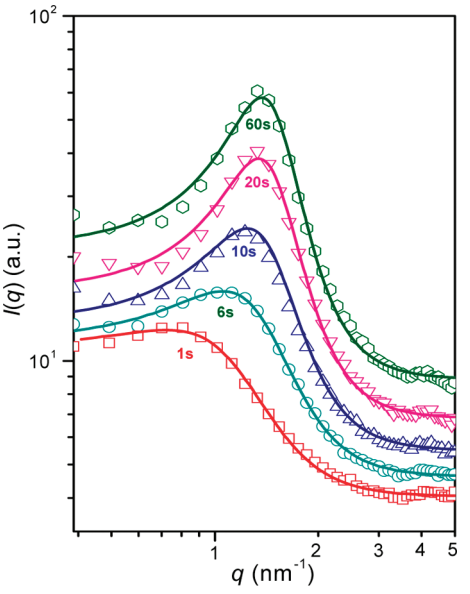

Figure 4. SAXS spectra of H_2O−MTSM−Teric G_9A_8 microemulsion with varying X-ray exposure time, full lines fit by eq 1. Scattering profiles of sample (b_4) at selected time points from Figure 3.

This functional form is simple and convenient for the fitting of the microemulsion SAXS spectra. Strey et al.[37−40] have extended the Teubner−Strey model for structured fluids in the disordered phase of the O/W/S system by defining the amphiphilicity factor (f_a) as a measure of the degree of order in the system:

$$f_a = \frac{B}{\sqrt{4AC}} \tag{5}$$

For intermediate amphiphilicity $-1 < f_a < 0$, a strongly structured, "good" microemulsion results. Increasing f_a (decreasing amphilicity, $0 < f_a < 1$) results in a poorly structured microemulsion.

Figure 4 shows fitting results for selected SAXS curves derived from Figure 3. As shown, the Teubner−Strey model describes the experimental scattering data well. As demonstrated by the coefficients between the calculated curves and the data, at the early stage of the polymerization, the fits are closer to the data than at the end of polymerization. This is perhaps not surprising, given that the Teubner−Strey model was developed specifically for microemulsions and not for polymerized materials. At the same time, the fits are surprisingly acceptable, and the fitted parameters from modeling the SAXS data can provide insight into the structural transitions during the microemulsion polymerization. Figure 5 shows the values of domain size d and correlation length ξ plotted as a function of X-ray exposure time. The microemulsion fitting parameters (d and ξ) drastically change over the first 20 s before reaching a plateau. This suggests that the polymerization is largely complete within this

time scale. The decrease in domain size (d) by 33% reflects a decrease in periodicity between oil and water domains, while correlation length, reflecting the degree of order in the polymerizable microemulsion, increased by 56% after polymerization. The decrease of d may be due to the volume changes (i.e., shrinkage) caused by solution−solid transition during the course of polymerization, resulting in the decrease of mean distance between domains. As for correlation length, the increased ξ value after polymerization reflects greater order in the solid phase. Meanwhile, the amphiphilicity factor f_a as calculated from eq 5 is also plotted in Figure 3, and it decreases sharply over the first 30 s but remains in the "good" microemulsion regime throughout the microemulsion polymerization process. Chen et al.[41] have reported that ξ/d is a measurement of the domain size polydispersity: the small the ratio, the larger the polydispersity. The value of ξ/d increased during the polymerization period, indicating that the microemulsion structure was constrained by cross-linking and the polydispersity of the domain size decreased.

In order to gain a deeper insight into the local structural changes, the core−shell model[25] was also chosen to interpret the scattering observed for the microemulsion polymerization and to provide further nanostructural detail about the system such as the droplet core radius and shell thickness. Using the SansView software, the microemulsion nanodroplets in this work were modeled as a dispersion of polydisperse spheres with a core−shell structure: the core is composed of water, cosurfactant (IPA), and surfactant hydrophilic groups, and the shell contains the surfactant hydrophobic groups and oil phase (MTSM). The broad peaks at $q \sim 1-2\ \mathrm{nm}^{-1}$, observed in the SAXS patterns are due to scattering from water droplets surrounded by surfactant

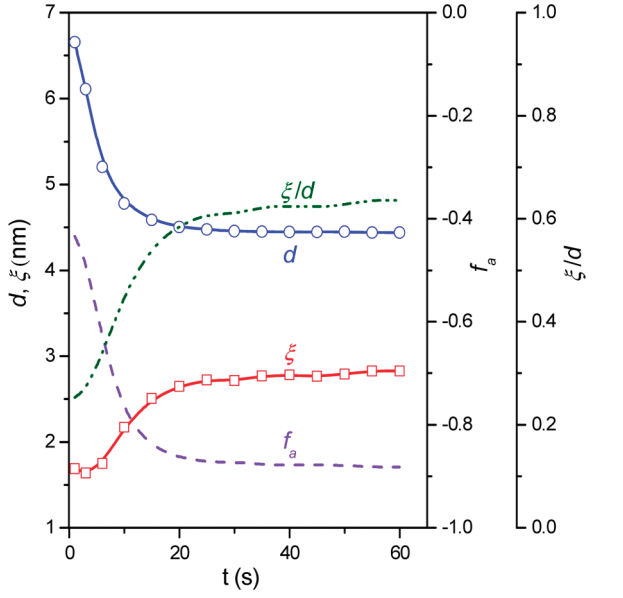

Figure 5. Variation of the microemulsion fit parameters (characteristic length scale of water domain, d, correlation length, ξ, and amphiphilicity factor, f_a, and domain size polydispersity, ξ/d) during microemulsion polymerization with increasing the X-ray exposure time based on Figure 3.

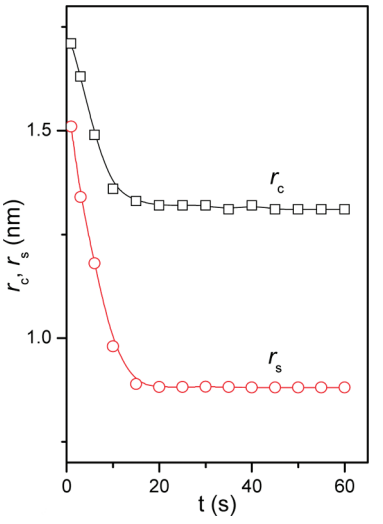

Figure 7. Variation of the microemulsion fit parameters (the radius of the shell, r_s, and the radius of the core, r_c) during microemulsion polymerization with increasing the X-ray exposure time based on Figure 3.

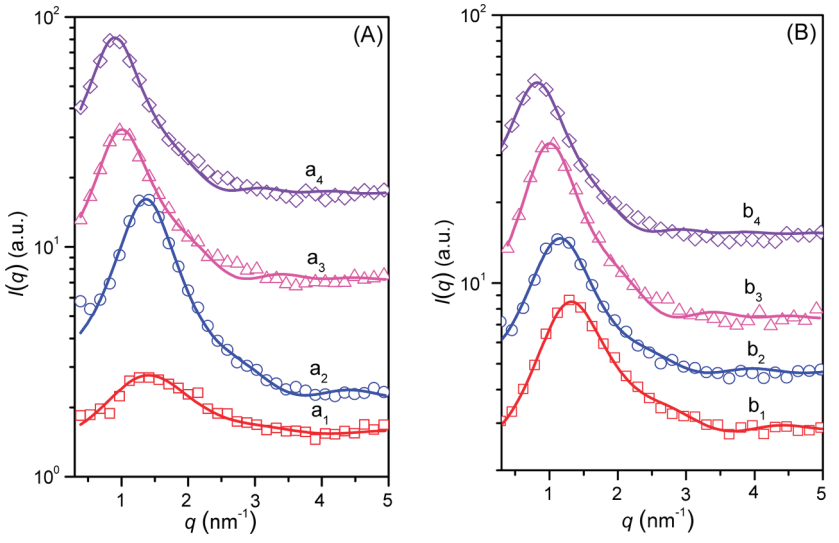

Figure 6. Scattering patterns of two sets of microemulsion: (A) microemulsion compositions along line (a) with increasing water content and (B) microemulsion compositions along line (b) with constant water content (15 wt %). The solid lines represent fits of the core−shell model to the data.

dx.doi.org/10.1021/ma102978u |*Macromolecules* 2011, 44, 3007–3015

Table 1. Structural Parameters Extracted from SAXS Analysis of the Microemulsion before and after Polymerization Using the Core−Shell Model

			core radius (r_c, nm)		shell thickness (r_s, nm)		polydispersity	
composition[a]	Φ_w (wt %)	$\Phi_{s/w}$	solution	polymerized	solution	polymerized	solution	polymerized
a_1	5	9.5	1.16	1.18	0.72	0.78	0.10	0.20
a_2	10	4.5	1.23	1.18	0.87	0.87	0.18	0.19
a_3/b_3	15	2.83	1.50	1.27	1.28	0.91	0.17	0.20
a_4	20	2	1.60	1.31	1.43	0.89	0.20	0.20
b_1	15	3.97	1.22	1.16	0.91	0.79	0.13	0.17
b_2	15	3.4	1.35	1.23	1.01	0.80	0.16	0.17
b_4	15	2.27	1.71	1.31	1.51	0.88	0.18	0.16

[a] The compositions of microemulsion are indicated in Figure 2.

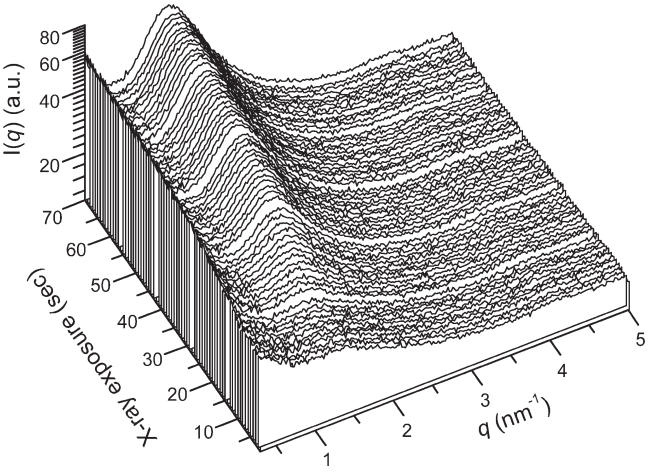

Figure 8. Time-resolved SAXS profiles of microemulsion composition (a_1) at varying polymerization time.

layer dispersed in the MTSM continuous phase. The total scattering intensity of a microemulsion system, $I(q)$, can be described as a function of the scattering vector:[20]

$$I(q) = n|\langle F(q)\rangle|^2\langle S(q)\rangle \quad (6)$$

where n is the number density of the scattering particles and the brackets, $\langle\ \rangle$ represent the ensemble average due to thermal fluctuations, $S(q)$ is the structure factor to indicate the correlation of the scattering elements, and $F(q)$ is the form factor, which describes the relation between the geometry of the scatterers and their scattering. The core polydispersity is taken into account by a probability function described by the Schulz distribution.[42] The form factor, $F(q)$, for a core−shell particle can be expressed by the following relation[43,44]

$$F(q) = V_c(\rho_c - \rho_s)F_0(qr_c) + V_s(\rho_s - \rho_{solv})F_0(qr_s) \quad (7)$$

where V_s is the volume of the outer shell, V_c is the volume of the core, r_s is the radius of the shell, ρ_c is the scattering length density of the core, ρ_s is the scattering length density of the shell, and ρ_{solv} is the scattering length density of the solvent. The function $F_0(x)$ is the first-order spherical Bessel function of the first kind.[20,45] The structure factor $S(q)$ in eq 6 was calculated assuming hard-sphere interaction based on the Percus−Yevick approximation.[46] The fitting of the scattering curves was performed using SANSview software with the values for the scattering length densities of the solvent (oil phase), core (H_2O), and shell (hydrophobic group of surfactant) of

Figure 9. Optically clear (a_1 and a_2) and opaque (a_3 and a_4) polymer membranes after UV polymerization.

$\rho_{solv} = 9.05 \times 10^{-4}$ nm^{-2}, $\rho_c = 9.47 \times 10^{-4}$ nm^{-2}, and $\rho_s = 9.03 \times 10^{-4}$ nm^{-2}, respectively. Other fitting parameters such as background, radius, scale factor, thickness, and core polydispersity were left as adjustable parameters used to fit the SAXS data.

Figure 6 shows fitting results for a series of microemulsion samples along line (a) and line (b) before polymerization. As can be seen, this model also describes our data well. Figure 7 shows the values of core radius (r_c) and shell thickness (r_s) from core−shell model fits plotted as a function of time. During polymerization, both r_c and r_s show sharp decreases during early time points, but after ~40 s they remain nearly unchanged, presumably indicating the completion of the X-ray-induced cross-linking. The decreasing trends of r_c and r_s are similar to the change of the domain size (d) of the Teubner−Strey model, and this indicates that the water droplets confined in the PDMS network shrink upon MTSM polymerization. This is consistent with the results presented by Waters and co-workers.[28] In their work, the PEG macromonomers functionalized with either acrylate or acrylamide end groups exhibited similar *in situ* SAXS patterns and the cross-link spacing of the PEG network decreased upon polymerization. In our case, we propose that the change in interfacial tension with respect to water in transitioning from monomer oil to solid polymer, combined with the decrease in volume of the cross-linked PDMS network results in the shrinkage of the confined water droplets.

Structural parameters derived from the core−shell model for a series of microemulsions with increasing water content (between 5 and 20 wt %, following line (a)) are presented in Table 1. As water content increases, both r_c and r_s increase. The water droplet swelling trend is consistent with the work presented by Glatter and co-workers.[47] This can be explained by the decrease of the ratio of surfactant to water ($\Phi_{s/w}$), an associated increased interfacial tension and lower interfacial area resulting in larger water droplets. The fitting results for the formulations along line (b) follow a similar trend, with decrease in the ratio of surfactant: MTSM at a

dx.doi.org/10.1021/ma102978u |*Macromolecules* 2011, 44, 3007–3015

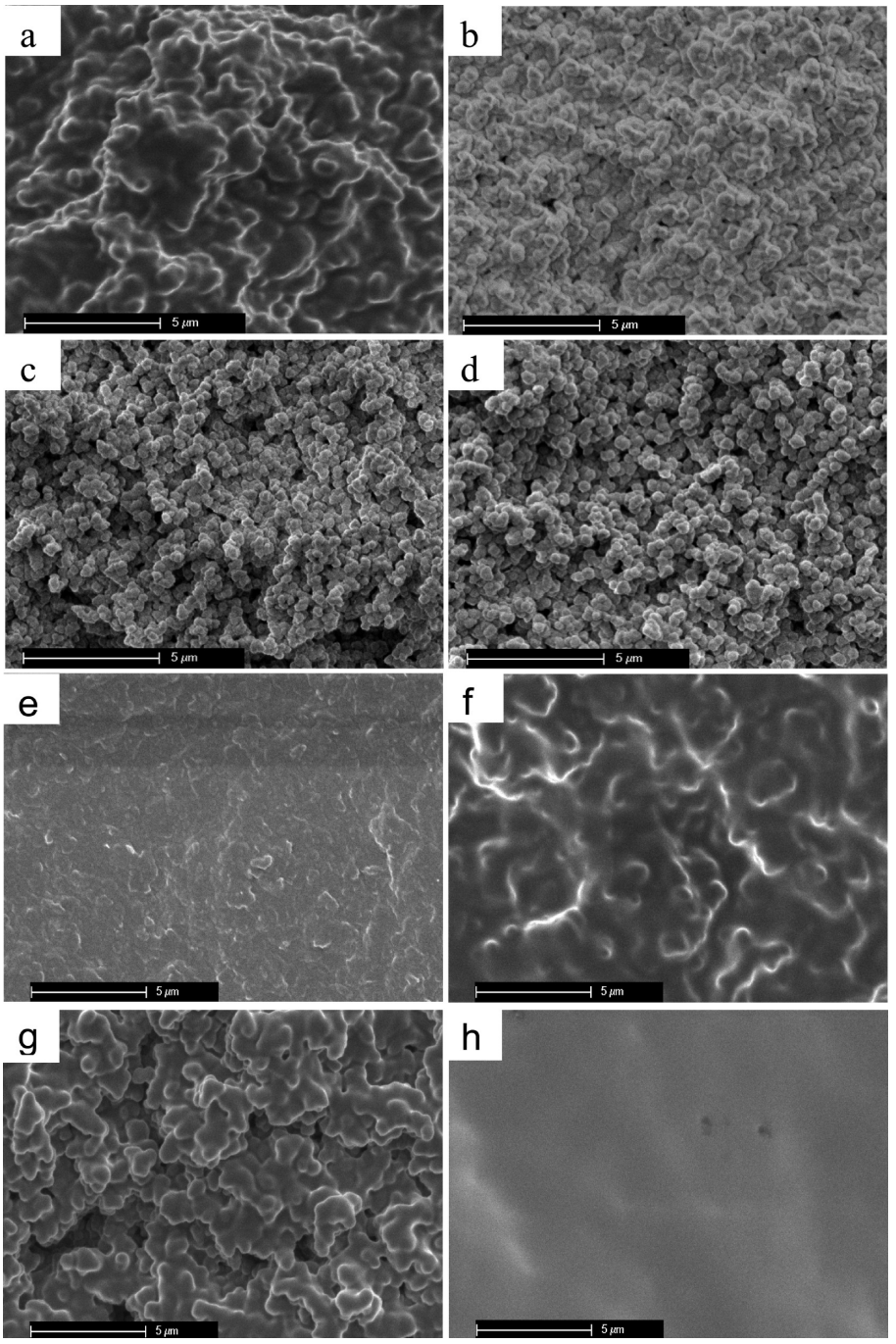

Figure 10. SEM images of the cross section of PDMS membranes and the corresponding precursor microemulsion compositions are indicted in phase diagram Figure 2: (a) b_1, (b) b_2, (c) b_3, (d) b_4, (e) a_1, (f) a_2, (g) a_4, and (h) along line (a) without water.

fixed water concentration (15 wt %), resulting in an increase of r_c and r_s. Upon polymerization of the microemulsion solutions by X-ray radiation, the SAXS data obtained from the polymers was still well described by the core−shell model, and the fitting results are also shown in Table 1. As can be seen, the values of r_c and r_s decreased upon polymerization in all cases except the compositions a_1 and a_2. Formulations a_1 and a_2 showed little change in r_c and r_s after polymerization, suggesting that the initial microemulsion structure was well preserved in these cases. This may be due to the high surfactant−water ratio in the precursor microemulsions a_1 and a_2. Microemulsion systems with a higher surfactant concentration may minimize the rearrangement of water domains during polymerization.[48] The time evolution of scattering curves during X-ray-induced polymerization of microemulsion a_1 is shown in Figure 8. The q_{max} values of these SAXS curves were almost identical during the course of polymerization, but the cross-linking of the oil phase gave rise to the increasing SAXS intensity.

Morphology of Polymerized Material. To visually investigate the morphology of polymerized material, a series of microemulsion compositions with different amounts of MTSM along lines (a and b) were selected for polymerization, and the

Scheme 2. Schematic Illustration of the Conceptual Model Describing the Transition from Microemulsion Solution to Solid Polymer with Different Surfactant Concentration: (A) at Low Surfactant Concentration; (B) at High Surfactant Concentration

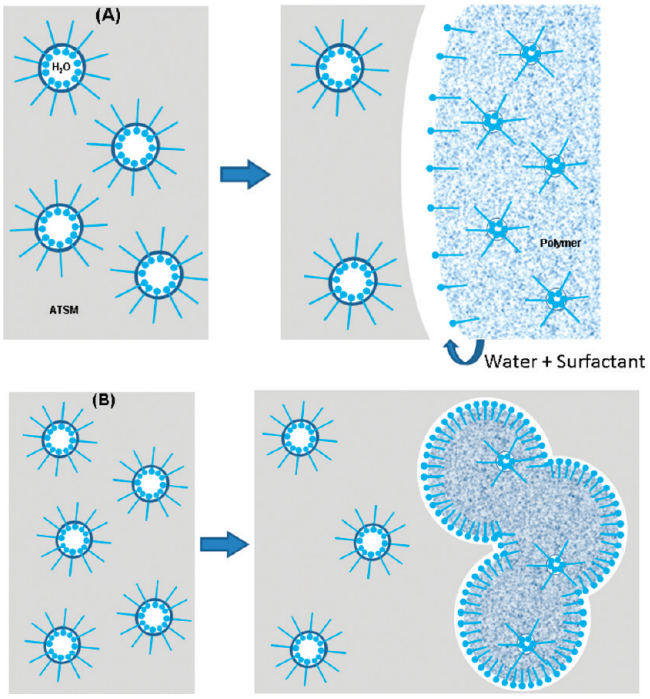

transparency of the resulting polymers was observed. Photographs of these samples are shown in Figure 9. As is shown in the figure, samples with higher surfactant concentration and lower water content exhibit increased transparency. The microscale morphology of the samples was also investigated using SEM. It should be noted that the samples for SEM study were cured by UV. A SAXS comparison of samples prepared using UV vs X-ray induced polymerization is presented in the Supporting Information. The data show that the two methods produced qualitatively similar nanostructure. Figure 10 shows the SEM images of UV polymerized samples. Qualitatively, samples with increased water content and decreased surfactant concentration exhibited increasingly discrete granular morphology. It seems likely that the appearance of granular morphology at higher water and lower surfactant content is the result of increased polymer particle size, resulting in increased scattering of light and hence opacity, as observed in Figure 9. Clearly, the changes in microemulsion nanostructure discussed above with respect to the SAXS analysis cannot explain these morphological variations, since they are manifested in the micrometer size range. We propose a conceptual model for explaining these morphological variations which is depicted in Scheme 2. As shown, in the fluid microemulsion solution, water droplets which are stabilized by the surfactant disperse in the continuous MTSM phase. The water droplets decrease with increasing surfactant concentration (see Table 1). During the course of polymerization, shrinkage of microemulsion droplets (see Figure 3) causes surfactant and water to be ejected from polymerizing material, and surfactant can further absorb at the new polymer–water/microemulsion interface. For formulations comprising lower surfactant concentration and higher water content, the interfacial tension at this new interface is higher, and the polymer particles are stabilized with a lower radius of curvature, resulting in larger polymer particles (granules). For higher surfactant concentrations (lower water content), the surfactant is able to reduce interfacial tension more effectively, resulting in higher radius of curvature and smaller polymer particles. While these smaller polymer particles were not discernible using SEM, we note that an earlier USANS study found some evidence for particles in the q range of 10^{-3}–10^{-2} nm^{-1} in a similar photopolymerizable system.[20]

CONCLUSIONS

A reactive methacrylate-terminated siloxane macromonomer (MTSM) was successfully synthesized for *in situ* microemulsion polymerization. The one-phase region of the ternary phase diagram for MTSM (oil phase), water, and a mixture of nonionic surfactant (Teric G_9A_8) with IPA (cosurfactant) was partially mapped at room temperature, enabling the preparation of inverse (oil in water) microemulsions. The time-dependent SAXS patterns during X-ray-induced polymerization of the microemulsions can be analyzed using the Tuebner–Strey model, and the results show that the periodicity of the oil and water domains decreased and correlation length increased during the polymerization, indicating shrinkage of the system. The analysis of the experimental SAXS patterns using the core–shell model suggested that the addition of water to the microemulsion system caused droplets within it to swell, in accordance with discontinuity of water in oil microemulsion. These water droplets shrank upon polymerization of the continuous oil phase when there was 15 wt % or more water in the precursor microemulsion solution. When there was 10 wt % or less water content in the precursor microemulsion, the rearrangement of water domains could be minimized during the course of polymerization and transparent polymerized material was obtained. The SEM analysis and visual observation revealed large differences in morphologies of polymerized materials from the microemulsion formulations with different water and surfactant contents. The polymerized materials with high water content and low surfactant concentration exhibited increasingly discrete granular morphology. A conceptual model based on the newly forming solid polymer–microemulsion interface was proposed to explain these morphological changes during the microemulsion fluid–polymer solid transition. This should be useful for tuning the final bulk properties of a polymerized material based on the starting microemulsion template composition and nanostructure.

ASSOCIATED CONTENT

Supporting Information. Figure S1. This material is available free of charge via the Internet at http://pubs.acs.org.

AUTHOR INFORMATION

Corresponding Author

*E-mail: qguo@deakin.edu.au (Q.G.); patrick.hartley@csiro.au (P.G.H.).

ACKNOWLEDGMENT

SAXS/WAXS research was undertaken at the Australian Synchrotron, Victoria, Australia, and the authors thank Dr. Nigel Kirby for his assistance. S.P. gratefully acknowledges the Deakin University and CSIRO for provision of a collaborative PhD scholarship and thanks M. Greaves (CSIRO) for assistance with

SEM experiments and D. Acharya (CSIRO) for assistance with SAXS measurements. We also thank Prof. G. Warr (University of Sydney) for helpful discussions with SAXS analysis.

REFERENCES

(1) Zana, R. *Adv. Colloid Interface Sci.* **1995**, *57*, 1–64.
(2) Danielsson, I.; Lindman, B. *Colloids Surf.* **1981**, *3*, 391–392.
(3) Stubenrauch, C.; Tessendorf, R.; Strey, R.; Lynch, I.; Dawson, K. A. *Langmuir* **2007**, *23*, 7730–7737.
(4) Hager, M.; Currie, F.; Holmberg, K. *Colloid Chem. II* **2003**, *227*, 53–74.
(5) Ingelsten, H. H.; Beziat, J. C.; Bergkvist, K.; Palmiqvist, A.; Skoglundh, M.; Hu, Q. H.; Falk, L. K. L.; Holmberg, K. *Langmuir* **2002**, *18*, 1811–1818.
(6) Hentze, H. P.; Kaler, E. W. *Curr. Opin. Colloid Interface Sci.* **2003**, *8*, 164–178.
(7) Texter, J.; Ge, L. H.; Mourey, T. H.; Bryan, T. G. *Langmuir* **2004**, *20*, 11288–11292.
(8) Pacios, I. E.; Renamayor, C. S. *J. Phys. Chem. B* **2009**, *113*, 16494–16500.
(9) Santhanalakshmi, J.; Anandhi, K. *Langmuir* **1996**, *12*, 3320–3325.
(10) Ho, B. S.; Tan, B. H.; Tan, J. P. K.; Tam, K. C. *Langmuir* **2008**, *24*, 7698–7703.
(11) Liu, J.; Gan, L. M.; Chew, C. H.; Teo, W. K.; Gan, L. H. *Langmuir* **1997**, *13*, 6421–6426.
(12) Palkovits, R.; Althues, H.; Rumplecker, A.; Tesche, B.; Dreier, A.; Holle, U.; Fink, G.; Cheng, C. H.; Shantz, D. F.; Kaskel, S. *Langmuir* **2005**, *21*, 6048–6053.
(13) Gao, F.; Ho, C. C.; Co, C. C. *J. Am. Chem. Soc.* **2004**, *126*, 12746–12747.
(14) Gao, F.; Ho, C. C.; Co, C. C. *Macromolecules* **2006**, *39*, 9467–9472.
(15) Co, C. C. *Soft Matter* **2008**, *4*, 658–662.
(16) Gaspar, L. J. M.; Baskar, G. *Biomacromolecules* **2006**, *7*, 1318–1322.
(17) Summers, M.; Eastoe, J.; Davis, S.; Du, Z. P.; Richardson, R. M.; Heenan, R. K.; Steytler, D.; Grillo, I. *Langmuir* **2001**, *17*, 5388–5397.
(18) Deen, G. R.; Gan, L. H.; Gan, Y. Y. *Polymer* **2004**, *45*, 5483–5490.
(19) Fu, X. A.; Qutubuddin, S. *Langmuir* **2002**, *18*, 5058–5063.
(20) Marszalek, J.; Pojman, J. A.; Page, K. A. *Langmuir* **2008**, *24*, 13694–13700.
(21) Tabor, R. F.; Eastoe, J.; Grillo, I. *Soft Matter* **2009**, *5*, 2125–2129.
(22) Hentze, H. P.; Co, C. C.; McKelvey, C. A.; Kaler, E. W. Templating vesicles, microemulsions, and lyotropic mesophases by organic polymerization processes. In *Colloid Chemistry 1*; Springer-Verlag: Berlin, 2003; Vol. 226, pp 197−223.
(23) N. Chan, G. Y.; Hughes, T. C.; McLean, K. M.; McFarland, G. A.; Nguyen, X.; Wilkie, J. S.; Johnson, G. *Biomaterials* **2006**, *27* (8), 1287–1295.
(24) Chaouk, H.; Wilkie, J. S.; Meijs, G. F.; Cheng, H. Y. *J. Appl. Polym. Sci.* **2001**, *80* (10), 1756–1763.
(25) Linder, P.; Zemb, T. *Neutrons, X-Rays and Light Scattering Methods Applied to Soft Condensed Matter*; Elsevier: Amsterdam, 2002.
(26) http://danse.chem.utk.edu/sansview.html.
(27) Collinson, E.; Dainton, F. S.; McNaughton, G. S. *Trans. Faraday Soc.* **1957**, *53*, 476–488.
(28) Waters, D. J.; Engberg, K.; Parke-Houben, R.; Hartmann, L.; Ta, C. N.; Toney, M. F.; Frank, C. W. *Macromolecules* **2010**, *43*, 6861–6870.
(29) Sharma, S. C.; Tsuchiya, K.; Sakai, K.; Sakai, H.; Abe, M.; Komura, S.; Sakamoto, K.; Miyahara, R. *Langmuir* **2008**, *24*, 7658–7662.
(30) Steytler, D. C.; Dowding, P. J.; Robinson, B. H.; Hague, J. D.; Rennie, J. H. S.; Leng, C. A.; Eastoe, J.; Heenan, R. K. *Langmuir* **1998**, *14*, 3517–3523.
(31) Teubner, M.; Strey, R. *J. Chem. Phys.* **1987**, *87*, 3195–3200.
(32) Atkin, R.; Warr, G. G. *J. Phys. Chem. B* **2007**, *111*, 9309–9316.
(33) Dave, H.; Gao, F.; Lee, J. H.; Liberatore, M.; Ho, C. C.; Co, C. C. *Nature Mater.* **2007**, *6*, 287–290.
(34) Regev, O.; Ezrahi, S.; Aserin, A.; Garti, N.; Wachtel, E.; Kaler, E. W.; Khan, A.; Talmon, Y. *Langmuir* **1996**, *12*, 668–674.
(35) Washburn, N. R.; Lodge, T. P.; Bates, F. S. *J. Phys. Chem. B* **2000**, *104*, 6987–6997.
(36) Hillmyer, M. A.; Maurer, W. W.; Lodge, T. P.; Bates, F. S.; Almdal, K. *J. Phys. Chem. B* **1999**, *103*, 4814–4824.
(37) Morkved, T. L.; Stepanek, P.; Krishnan, K.; Bates, F. S.; Lodge, T. P. *J. Chem. Phys.* **2001**, *114*, 7247–7259.
(38) Schubert, K. V.; Strey, R. *J. Chem. Phys.* **1991**, *95*, 8532–8545.
(39) Schubert, K. V.; Strey, R.; Kline, S. R.; Kaler, E. W. *J. Chem. Phys.* **1994**, *101*, 5343–5355.
(40) Koehler, R. D.; Schubert, K. V.; Strey, R.; Kaler, E. W. *J. Chem. Phys.* **1994**, *101*, 10843–10849.
(41) Chen, S. H.; Chang, S. L.; Strey, R. On the Interpretation of scatering Peaks from Bicontinuous Microemulsions. In *Trends in Colloid and Interface Science IV*; Zulauf, M., Lindner, P., Terech, P., Eds.; Dr. Dietrich Steinkopff Verlag: Berlin, 1990; Vol. 81, pp 30−35.
(42) Kotlarchyk, M.; Chen, S.-H. *J. Chem. Phys.* **1983**, *79*, 2461–2469.
(43) Guinier, A.; Fournet, G. *Small Angle Scattering of X-Ray*; Wiley: New York, 1955.
(44) Carnali, J. O.; Fowkes, F. M. *Langmuir* **1985**, *1*, 576–587.
(45) Megens, M.; van Kats, C. M.; Bösecke, P.; Vos, W. L. *Langmuir* **1997**, *13* (23), 6120–6129.
(46) Percus, J. K.; Yevick, G. J. *Phys. Rev.* **1958**, *110*, 1–13.
(47) Glatter, O.; Orthaber, D.; Stradner, A.; Scherf, G.; Fanun, M.; Garti, N.; Clement, V.; Leser, M. E. *J. Colloid Interface Sci.* **2001**, *241*, 215–225.
(48) Chieng, T. H.; Gan, L. M.; Chew, C. H.; Lee, L.; Ng, S. C.; Pey, K. L.; Grant, D. *Langmuir* **1995**, *11*, 3321–3326.